Ab-initio design of nanophotonic waveguides for tunable, bidirectional optical forces

Favuzzi, Pedro A.; Bardoux, Richard; Asano, Takashi; Kawakami, Yoichi; Noda, Susumu

Ab-initio design of nanophotonic waveguides for tunable, bidirectional optical forces

Pedro A. Favuzzi,* Richard Bardoux, Takashi Asano, Yoichi Kawakami and Susumu Noda

Department of Electronic Science and Engineering, Kyoto University, Kyoto 615-8510, Japan

*pedro.favuzzi@optomater.kuee.kyoto-u.ac.jp

Abstract: We propose a set of principles to tailor and enhance optical forces between parallel, periodic dielectric waveguides by molding the eigen-mode field distribution via the combined effects of highly symmetric slow light modes and waveguide morphology. The geometries here considered are amenable to standard lithographic techniques and possess strong repulsive and attractive optical forces that can be enhanced via slow-light band edge modes. This new methodology should enable the fabrication of optomechanical devices for applications in sensing, switching and nano-optomechanical systems.

OCIS codes: (250.0250) Optoelectronics; (130.5296) Photonic crystal waveguides; (250.5300) Photonic integrated circuits; (350.4238) Nanophotonics and photonic crystals; (120.4880) Optomechanics.

References and links

1. J. D. Jackson, *Classical Electrodynamics*, 3rd ed (Wiley, 1998).
2. D. V. Thourhout and J. Roels, "Optomechanical device actuation through the optical gradient force," Nat. Photonics **4**, 211–217 (2010).
3. M. Bagheri, M. Poot, M. Li, W. Pernice, and H. Tang, "Dynamic manipulation of mechanical resonators in the high amplitude regime through optical backaction," Nature Nanotech. **6**, 726–732 (2011).
4. M. Aspelmeyer, S. Groblacher, K. Hammerer, and N. Kiesel, "Quantum optomechanics–throwing a glance," J. Opt. Soc. Am. B **27** 189–197 (2010).
5. J. Ma and M. Povinelli, "Applications of optomechanical effects for on-chip manipulation of light signals," Curr. Opin. Sol. State Mater. Sci **,**16 82–90 (2012).
6. M. Povinelli, M. Loncar, M. Ibanescu, E. Smythe, S. Johnson, F. Capasso, and J. Joannopoulos, "Evanescent-wave bonding between optical waveguides," Opt. Lett. **,**30 3042–3044 (2005).
7. M. Li, W. Pernice, and H. Tang, "Tunable bipolar optical interactions between guided lightwaves," Nat. Photonics **3**, 464–469 (2009).
8. A. Oskooi, P. Favuzzi, Y. Kawakami, and S. Noda, "Tailoring repulsive optical forces in nanophotonic waveguides", Opt. Lett. **36**, 4638–4640 (2011).
9. M. Eichenfield, J. Chan, R. Camacho, K. Vahala, and O. Painter, "Optomechanical crystals," Nature **462**, 78–82 (2009).
10. J. Ma and M. Povinelli, "Effect of periodicity on optical forces between a one-dimensional periodic photonic-crystal waveguide and an underlying substrate," Appl. Phys. Lett. **97** (2010).
11. J. D. Joannopoulos, S. G. Johnson, R. D. Meade, and J. N. Winn, *Photonic Crystals: Molding the Flow of Light*, 2nd ed (Princeton Univ. Press, 2008).
12. S. G. Johnson and J. D. Joannopoulos, "Block-iterative frequency-domain methods for Maxwell's equations in a planewave basis," Opt. Express **8**, 173–190 (2001).
13. V. Almeida, Q. Xu, C. Barrios, and M. Lipson, "Guiding and confining light in void nanostructure," Opt. Lett. **29**, 1209–1211 (2004).

#173207 - $15.00 USD Received 24 Jul 2012; revised 21 Sep 2012; accepted 25 Sep 2012; published 11 Oct 2012

14. E. Gavartin, R. Braive, I. Sagnes, O. Arcizet, A. Beveratos, T. J. Kippenberg, and I. Robert-Philip, "Optomechanical coupling in a two-dimensional photonic crystal defect cavity," Phys. Rev. Lett. **106**, 203902 (2011).
15. M. Tinkham, *Group Theory and Quantum Meachanics*, 2nd ed (Dover, 1992).

1. Introduction

Optical forces are due to momentum exchange between photons and their surrounding media [1]. Recently, optical forces are being investigated in nanostructures for possible applications in sensing, switching and other nanoelectromechanical systems (MEMS) [2,3]; most work being focused in the photon-phonon quantum domain [4]. In the classical regime, where larger mechanical displacements can be induced and most near-term technologies are expected [5], possible applications have been hindered by the weak *and* mainly attractive character [6, 7] of such forces. To address these shortcomings we previously showed that repulsive optical forces between parallel waveguides with uniform cross section can be enhanced via careful morphological considerations [8]. Nevertheless, due to the shape of the proposed waveguide [8], experimental observation of such forces would require either manual alignment of two half-cut, tapered optical fibers, or use of complex three dimensional (3D) stereographic techniques. Here we demonstrate that the same behavior can be observed in waveguides having periodic modulation along the propagation axis (3D system), that are amenable to fabrication via commonly-used lithographic (2D) techniques. More over, to explain such behavior, we develop a framework by means of a more-refined formulation of the optical force [9], which directly connects the sign and magnitude of the force to the field distribution. This semi-empirical method can be used to ab-initio tailor optical forces between parallel waveguides with constant cross-section along the axis (2D system) by engineering the electric field distribution via careful choice of the waveguide's morphology. Most importantly it can be consistently extended to 3D systems, where the field distribution over the 3D unit cell can be studied, as we will demonstrate, via slow light modes. In fact, highly-symmetric band-edge modes can not only be used to enhance the absolute field intensity along the waveguide [8,10], but also to analyze and tailor the electric field distribution itself.

2. Forces between photonic waveguides

Optical forces are usually measured by the Maxwell Stress Tensor [1] or energy-conservation based approaches [6], which do not yield useful insights into how the eigenmode field distribution gives rise to the resulting force. To visualize such interaction we use a formulation of optical forces originally developed to analyze the photon-phonon coupling in the semi-classical regime [9] that, for a non-deformable media, can be written as:

$$\frac{\mathbf{F}}{U} = \frac{\int_A \frac{\Delta\varepsilon}{2}\left(\left|E_{\parallel}\right|^2 + \frac{1}{\varepsilon_1\varepsilon_2}\left|D_{\perp}\right|^2\right)\mathbf{n}\,dA}{\int_V \varepsilon\left|E\right|^2 dV}, \tag{1}$$

where A denotes the surface of the waveguide, $U = N\hbar\omega$ is the total electromagnetic energy per unit cell (coupled into a propagative eigenmode of frequency ω), ε_1 and ε_2 are the permittivity of the waveguide and surrounding medium, respectively, $\Delta\varepsilon = \varepsilon_1 - \varepsilon_2$, $\mathbf{n}$ is a dimensionless unit-vector normal to the surface of integration, always directed from the high to the low dielectric index regions, and $E_{\parallel}$ and $D_{\perp}$ are the electric field parallel and displacement field normal to A. More precisely, $\mathbf{E}$ is the electric field of the fundamental, orthonormal ($\int_V \varepsilon\mathbf{E_i}\cdot\mathbf{E_j}dV = \delta_{ij}$, V is the unit-cell volume) mode propagating along two parallel waveguides. More over, $\mathbf{E}$ is symmetric respect to a mirror transformation about the x-y plane (z-symmetry), the x-z plane

#173207 - $15.00 USD Received 24 Jul 2012; revised 21 Sep 2012; accepted 25 Sep 2012; published 11 Oct 2012

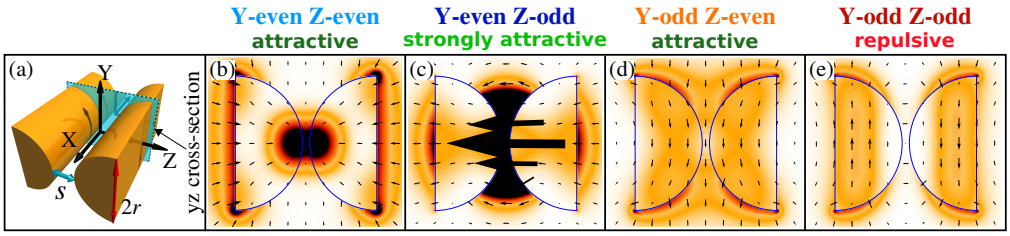

Fig. 1. **(a)** Schematics of the geometry in use. **from (b) to (e)**: In-plane $\mathbf{E_{yz}}$ vector-field distribution (larger arrows mean more intense) with the total $|E|^2$ in the background (darker is more intense) for the four fundamental modes of parallel waveguides with a semicircle profile ($r = a/2$) at an axial wave-vector of π/a and a fixed distance $s = 0.05a$. All arrows lengths and color scales share the same normalization.

(z-symmetry) and translationally symmetric along the x-axis as shown in Fig. 1. It follows that the total force acting on the single waveguide is parallel to the z-axis with respectively opposite directions for each of the two waveguides. For simplicity, we only consider the rightmost waveguide in Fig. 1(a), for which "attractive" forces (approaching waveguides) are negative and a "repulsive" forces are positive. We can now simplify Eq. (1) from vectorial to scalar form, since its direction is known, by substituting $\mathbf{n}$ with its projection along the z-axis as $(\mathbf{n}\cdot\mathbf{z})$, where $\mathbf{z}$ is the z-axis unit vector. Equation (1) shows that the sign of the force depends only on the field distribution along these two waveguide boundaries: fields localized along the "*inner*" surfaces, along which the dot product $\mathbf{z}\cdot\mathbf{n}$ is negative, will contribute to an *attractive* force, while those along the"*outer*" ones (for which $\mathbf{z}\cdot\mathbf{n} > 0$) will be *repulsive*. Here we present *five* principles based on the variational theorem [11] and Eq. (1) that can be used to *infer* and tailor the direction and relative amplitude of optical forces via an educated guess of the field distribution for a given mode and geometry; enabling us to tailor optical forces in 2D and 3D systems. In order to consistently evaluate the force for different shapes, modes and group velocities, the force is normalized by U, instead of the mode *power*, that would bear a force inversely proportional to the group velocity (v_g) [6, 8] . It follows from the given definition of $\mathbf{E}$ and the arbitrariness of U (assumed constant and set to unity for all systems) that the denominators on both sides of Eq. (1) can be neglected without loss of generality.

3. Intuitive description of the electric field behavior

To intuitively introduce all five principles of our ab-initio design procedure, we examine two parallel semicircular (of diameter a), Silicon (refractive index, $n = 3.45$) waveguides shown in Fig. 1(a). Such design was specifically chosen to achieve strong repulsive forces for any arbitrary separation [8], but, as an example, we only look at a fixed-separation of $s = 0.05a$. Besides the two "symmetric" and "anti-symmetric" guided-modes [2, 6, 8] (defined by the y-odd/z-even(OE) and y-odd/z-odd(OO) symmetries, we also study the y-even/z-even(EE) and y-even/z-odd (EO) guided-modes, in order to provide a complete treatment. The field normalization (vector lengths and color scale), used in Fig. 1, is identical for all modes, which permits a valid comparison of the relative force strength by means of Eq. (1).

First, we know from the variational theorem, as extensively discussed in literature [12], that a general tendency of the fundamental mode is to concentrate $\mathbf{E}$ within the waveguides while trying to reduce its spatial variations [8]. It follows two competitive effects: the fields will tend to cross at normal incidence or parallel to the waveguide's surface, and, at the same time, those components of $\mathbf{E}$ localized in the air regions will tend to have a smaller magnitude compare to components localized inside the waveguides.

#173207 - $15.00 USD Received 24 Jul 2012; revised 21 Sep 2012; accepted 25 Sep 2012; published 11 Oct 2012

Second, when a given set of symmetries is applied, more stringent conditions need to be considered: any symmetry will *repel* those field's components with a node over the mirror plane and *localize* the remaining ones along such plane. An example, in combination with the first principle, is the well-known slot-waveguide (SW) effect [13], which can arise if an odd-symmetry mirror is located between two high dielectric index regions separated by a small gap. This effect can be observed in Fig. 1(c): the EO mode shows a large confinement of the E_z component (large black arrows) in the narrow, void region separating the waveguides that induces a strong, attractive force.

Third, the chosen symmetries define the relative magnitude of each field component: most of the mode energy will be carried by the component of E with the lesser number of *symmetry-induced* nodes over the unit cell. For example, the OE mode (Fig. 1(d)) behavior is dominated by E_y since the y-odd and z-even symmetries induce no nodes for that field component. As a result the field is mainly localized between the two waveguides inducing an attractive force. We would like to notice that accidental nodes (usually single points in 2D or lines in 3D) where one or more components have zero magnitudes do not have to be considered.

Fourth, at the same intensity, the force induced by the $E_\perp$ (measured inside the high dielectric index region) is $\varepsilon_1/\varepsilon_2$ times larger than the force induced by $E_\parallel$. The EE mode (Fig. 1(b)) is attractive due to a marked localization of E_x (third principle) between the waveguides, yet the force is smaller relatively to the EO mode as the attraction is offset by the repulsive contribution of the vertical E_z component along the outer boundary which is enhance by a factor of $\varepsilon_1/\varepsilon_2$ even if the magnitude of E_z (not even visible in Fig. 1(b)) is much smaller that E_x.

Fifth, according to Eq. (1), since we are only interested in the component of the force parallel to the z-axis, those regions where the surfaces are mostly oriented toward the y-axis ($\mathbf{z}\cdot\mathbf{n}\approx 0$) have a reduced contribution to the total force proportional to $\mathbf{z}\cdot\mathbf{n}$ itself. For example the OO mode (Fig. 1(e)) induces a repulsive force as the fields along the inner surfaces are mainly localized at the very tip of the semicircle, where $\mathbf{z}\cdot\mathbf{n}$ is small, while the fields along outer surfaces fully contribute to the force.

4. Predicting the electric field configuration

In order to apply these principles, we propose the following recursive recipe.

Step one, we choose a set of symmetries and, with no regard for the shape of the waveguide, we fix the global modal field distribution via the second principle. The main goal is to determine the position of each field component respect to the symmetry planes. We notice that, unless we change the symmetries, no geometry can change such distribution.

Step two, we superimpose the chosen geometry to the fields and, by following the third and first principle, we deduce the field pattern with respect to the waveguide and the relative magnitude of each **E** component. In fact, while in step one we consider no interaction between the fields and the waveguide's geometry, via the first principle, if guided modes are considered, it is possible to pin the field distribution to the waveguide geometry. With the third principle, the relative magnitude between the different components of **E** is fixed. Once this is done we have to check the fields for consistency with the first principle. For example, if the mode's dominant component were localized in air, according to the third principle other field components that are localized in the high dielectric index region might be enhanced instead. In addition, components that can induce a SW effect are often favored by the first principle, and, as a rule of thumb, we assume that the SW effect always dominates the mode's behavior. In some cases, however, it is possible to suppress such effect by a proper choice of waveguide geometry. In Fig. 1(e) rounded inner walls were used to increase the spatial variations of the SW effect as we move away from the origin (where SW is suppressed by the y-even symmetry), along the y-axis. For fairness we would like to mention that, while not necessary, it is useful to have an example

#173207 - $15.00 USD Received 24 Jul 2012; revised 21 Sep 2012; accepted 25 Sep 2012; published 11 Oct 2012

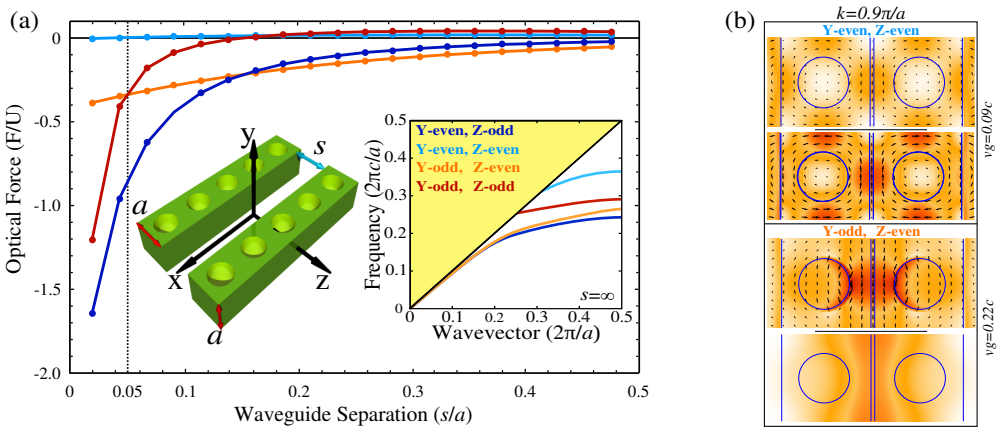

Fig. 2. **(a)** Normalized force per unit energy as a function of the waveguide-separation distance s/a of the four fundamental slow-light modes ($k_x = 0.98\pi/a$) of two parallel-waveguides shown in inset (periodicity a, radius $0.3a$). The inset also shows the dispersion diagram of the four studied modes. **(b)** Field distribution ($y = 0$ and $y = 0.47a$ from the bottom) of the y-even/z-even and y-odd/z-even modes at the wavevector $k_x = 0.9\pi/a$

where the exact **E**-field is known. This is specially important when analyzing very different axial-wavevectors (k_x) and materials, since the mode confinement in the high dielectric index regions and the coupling between the two waveguides depends on the relation between the waveguide's cross-sectional area, refractive index and and k_x.

Step three, we apply the fourth and fifth principles and evaluate direction and magnitude of the force. This step is essential to a proper choice of geometry and symmetry. While here, for simplicity, we only treat attractive and repulsive forces, this frame work can be applied to complex mechanical vibrational modes [14], where a large superposition of the mechanical and electromagnetic modes can induce a significant increase in optomechanical coupling.

Finally, if the resulting force does not agree with our requirements, we can either change the symmetries and/or waveguide's geometry in order to eliminate, as we will show later, those regions over which the force is applied, or change the field themselves [8]; repeating the procedure until a proper geometry and symmetries are found.

5. Forces between periodic waveguides

We now want to extend our method to periodic, coupled waveguides, where the fields need to be considered over the full 3D unit cell. In this case our method would often (but not always) fail to describe the attractive or repulsive nature of the optical modes, since the field distribution along the propagation axis cannot be described with only two symmetry planes. If a third symmetry plane were to be found, the extension of our method to 3D is straightforward. We do so via slow light modes, that have been previously used to markedly enhance the magnitude of the force [8, 10], as the field energy is inversely proportional to v_g (via $U = LP/v_g$) [11]. In fact, at $k_x = \pi/a$ (a is the length of the periodicity) the Bloch plane-wave, envelope function regains the symmetry along the x-axis; so does the Hermitian eigenproblem [15] and, as a consequence, the E-field becomes symmetric as well (if the geometry considered is symmetric along the x-axis). More over, for any given mode, once small enough values of v_g have been reached (we observe no important changes for $v_g < 0.15c$, where c is the speed of light in vacuum), further reductions of v_g will not significantly alter such mode's **E**-field *distribution* in the unit cell: in fact v_g is given by $v_g = d\omega/dk_x$ and, as the Brillouin-zone boundary is approached, the eigenfrequency

#173207 - $15.00 USD Received 24 Jul 2012; revised 21 Sep 2012; accepted 25 Sep 2012; published 11 Oct 2012

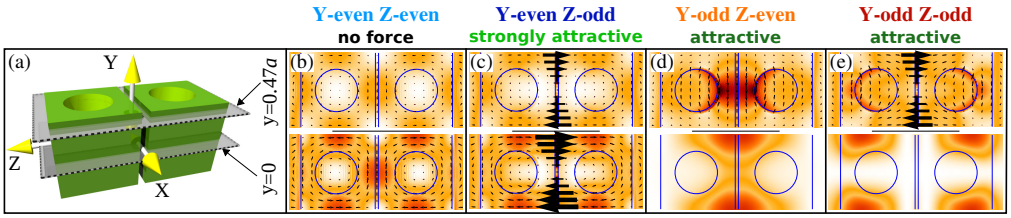

Fig. 3. **(a)** Waveguide's unit cell. **From (b) to (e)**: In plane $\mathbf{E_{zx}}$ vector-field distribution (larger arrows mean more intense) with the total $|E|^2$ in the background (darker is more intense) for the four fundamental modes of parallel periodic waveguides (periodicity a, radius $0.3a$, separation $s/a = 0.05$) cut along $y = 0$ and $y = 0.47a$ at $k_x = 0.98\pi/a$. Arrows and colors of all figures share the same normalization.

and by extension the eigenmode itself changes less and less (as they are inextricably linked through the variational theorem). This therefore enables us to analyze the field profile of modes slightly offset from the band edge, which can be experimentally probed. As a first example we look at a commonly use 3D periodic waveguide with cylindrical, periodic holes. Forces, fields and schematic of the geometry are shown in Fig. 2 and 3. We can see from Fig. 2(b) that the field distribution of the EE mode, at $v_g = 0.09c$, shows no change from $k_x = 0.90\pi/a$ to $k_x = 0.98\pi/a$ ($v_g = 0.02c$, shown in Fig. 3(b)); while, the OE mode, associated to a larger v_g at $k_x = 0.90\pi/a$ (inset of Fig. 2(b)), shows visible (even if the general features remain) changes from the corresponding fields at $k_x = 0.98\pi/a$ and $v_g = 0.14c$ (Fig. 3(d)).

From Fig. 2 we notice that, for this particular geometry, none of the four modes exhibits strong repulsive forces. Such behavior is fully justified by the geometry in use: in fact, no matter what the parity of the x-mirror symmetry might be, a fast analysis via the method discussed above will demonstrate that strong repulsive forces cannot appear. In Fig. 3 we show the field distributions of each eigenmode in the middle and near the top of the unit cell (cross section in the xz-plane), which should be sufficient for revealing its main features as the fields vary continuously. While EO and OE modes behave similarly to their 2D counterparts, the OO and the EE modes deserve a more detailed explanation as both modes can be used to induce strong repulsive forces if a proper geometry is chosen. At short distances the OO mode is attractive due to the presence of a SW effect while is repulsive at large separations where E_y dominates. The field distribution of the EE mode is a consequence of the band-edge induced x-mirror. With our method we first study EE at large separations. From step one and the first part of step two we notice that E_x is localized along the z-axis, where the low dielectric index air-hole is present, and E_z (repelled by z-even and x-odd while promoter by y-even) is mainly localized inside the lateral high dielectric index regions. From the last part of step two, we would at first expect E_x to dominate, however from the third principle we would soon realize that, since E_x is mainly localized in air, an enhancement of the magnitude of E_z is expected. Moreover, we also expect E_x to be localized along the small dielectric bridges around the air hole, with a preference for flat surfaces (through which E_x can cross continuously). In conclusion, since the E_x field is well balanced between inner and outer regions, the effect is dominated by the E_z component; inducing a very weak repulsive force (Fig. 2(a)). However, as the two waveguides come closer together (Fig. 3(b)), the increasing amount of dielectric at the origin allows E_x to increase its presence at the center of the unit cell, therefore inducing an extremely-weak, attractive force (negligible at $s/a = 0.05$).

#173207 - $15.00 USD Received 24 Jul 2012; revised 21 Sep 2012; accepted 25 Sep 2012; published 11 Oct 2012

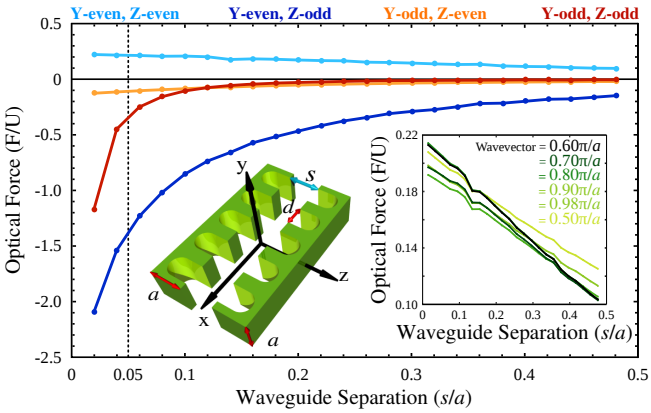

Fig. 4. Normalized force per unit energy as a function of the waveguide-separation distance s/a for the four fundamental slow-light modes ($k_x = 0.98\pi/a$) of two parallel-waveguides shown in inset (periodicity a, diameter $d = 0.6a$).The inset also shows the normalized force of the y-even/z-even mode for several different wavevectors.

6. Tailoring optical forces via morphology and slow light

We use the EE mode to demonstrate the validity of our method. We notice from step three that the attractive effect of E_x is induced along the dielectric bridges closer to the z-symmetry plane. If we remove them (the new geometry is shown in Fig. 4(b)), from step two, the EE mode should be dominated by E_x because of the presence of a SW effect and the distribution of E_x over the remaining dielectric bridge should be unchanged. By applying step three to this geometry we notice that, even if most of the energy is localized at the center of the unit cell, where no dielectric walls are present, no attractive force can be induced. As a consequence, the total force over the unit cell is repulsive. Our predictions are confirmed by Fig. 4 where it can be observed that the EE mode exhibits a monotonically growing repulsive force as the distance between the two waveguides is reduced, while the behavior of the remaining modes is consistent with our model. The EO and OO modes, in fact, exhibits no significant change since the SW effect (E_z), as shown in Fig. 3, was already pushed toward the edge of the unit cell by the x-odd symmetry, while the magnitude of the attractive force induced by OE mode is reduced roughly by half due to the reduced amount of dielectric at the center of the unit cell as shown in Fig. 5(d). The EE's attractive force is stronger when the two waveguides are in contact, however we only measure forces up to a minimum separation of $s/a = 0.02$ since, at $s = 0$ Eq. (1) it is not properly defined. At $s/a = 0.02$ the repulsive force induced by the EE mode shown in Fig. 4 is 5.8 and 17.9 times larger compared to the strongest repulsive forces ($s/a = 0.34$) shown in Fig. 2, calculated for the OO and EE modes, respectively. As separation is increased, the force of the EE mode in Fig. 4 gradually decreases but, at $s/a = 0.34$, only a 40% reduction from its peak force is observed. In physical units this is equal to (per unit cell, with $n = 3.45$ at a wavelength $\lambda = 1.55\ \mu m$, assuming a realistic value of $v_g = 0.01c$, an input power of $P = 0.1\ W$ at $s/a = 0.34$) a repulsive and attractive force of $F = 4.5\ nN$ (EE mode) and $F = -7.6\ nN$ (EO mode), respectively. These values are similar to those we previously reported [8], where, for the same parameters, a repulsive and attractive force of $F = 4.8\ nN$ (OO mode) and $F = -3.9\ nN$ (OE mode) were observed, albeit with geometries not amenable to fabrication by simplelithographic techniques.

#173207 - $15.00 USD Received 24 Jul 2012; revised 21 Sep 2012; accepted 25 Sep 2012; published 11 Oct 2012

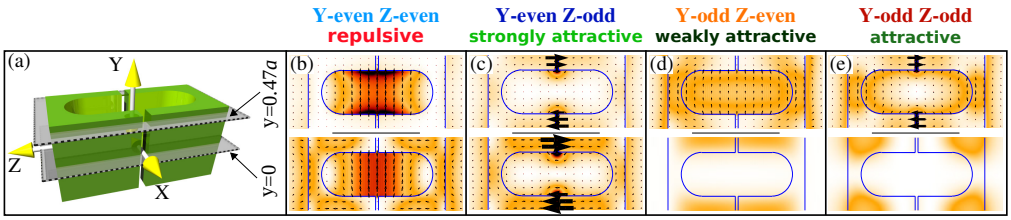

Fig. 5. **(a)**: Waveguide's unit cell. **From (b) to (e)**: In plane $\mathbf{E_{zx}}$ vector-field distribution (larger arrows mean more intense) with the total $|E|^2$ in the background (darker is more intense) for the four fundamental modes of parallel waveguides (periodicity a, radius $0.3a$, separation $s/a = 0.05$) cut along $y = 0$ and $y = 0.47a$ at $k_x = 0.98\pi/a$. Arrows and colors of all the figures share the same normalization.

7. Conclusions

By following the same principles here discussed we have found structures that, while always feasible to conventional fabrication processes, exhibit strong repulsive forces by, for example, suppressing the SW effect commonly associated with the OO mode. More over, in 3D systems, the same method can be easily extended to the four, fundamental modes (given by x-odd) or to the analysis of other resonant structures. In conclusion we have demonstrated and described a methodology to ab-initio tailor optical forces between nanophotonic waveguides via careful design of the waveguide morphology through specific symmetry constrains and, when periodicity is introduced, via band-edge modes. As a result the geometries considered exhibit strong repulsive and attractive forces while being amenable to fabrication via standard lithography techniques. While this method is no substitute of a rigorous eigenmode calculations, it avoids blind optimization of the waveguide geometry and should help find geometries and tools to develop novel optomechanical applications.

Acknowledgments

One of the authors (P. A. F.) would like to thank Jeremy Upham and Mian Wang for the useful comments and discussions.

#173207 - $15.00 USD Received 24 Jul 2012; revised 21 Sep 2012; accepted 25 Sep 2012; published 11 Oct 2012